

REPORT DOCUMENTATION PAGE

AFRL-SR-BL-TR-98-

Public reporting burden for this collection of information is estimated to average 1 hour per response, including the time for reviewing the data needed, and completing and reviewing the collection of information. Send comments regarding this burden estimate or any other aspect of this collection of information, including suggestions for reducing this burden, to Washington Headquarters Services, Directorate for Information Operations and Reports, 1215 Jefferson Davis Highway, Suite 1204, Arlington, VA 22202-4302, and to the Office of Management and Budget, Paperwork Reduction Project (0704-0188), Washington, DC 20503.

therring
tion of
r, Suite

DS/B

1. AGENCY USE ONLY (Leave Blank)	2. REPORT DATE January 1997	3. REPORT TYPE AND DATES COVERED Final (01 Jan 94 - 31 Dec 96)	
4. TITLE AND SUBTITLE A Study of Stability and Energy Conservation of a 3-D Electromagnetic PIC Code for Non-Orthogonal Meshes		5. FUNDING NUMBERS F49620-94-1-0336	
6. AUTHORS Dmitri Kondrashov, Joseph Wang, Paulette C. Liewer			
7. PERFORMING ORGANIZATION NAME(S) AND ADDRESS(ES) California Institute of Technology Pasadena, CA 91125		8. PERFORMING ORGANIZATION REPORT NUMBER	
9. SPONSORING/MONITORING AGENCY NAME(S) AND ADDRESS(ES) AFOSR/NM 110 Duncan Avenue, Room B-115 Bolling Air Force Base, DC 20332-8080		10. SPONSORING/MONITORING AGENCY REPORT NUMBER	
11. SUPPLEMENTARY NOTES			
12a. DISTRIBUTION AVAILABILITY STATEMENT Approved for Public Release		12b. DISTRIBUTION CODE	
13. ABSTRACT (Maximum 200 words) A 3-D electromagnetic particle-in cell code (EMPIC) was developed for large-scale plasma simulation on parallel computers. To simulate plasma problems with complex geometries such as high-power microwave generation devices, curvilinear coordinates were used. A logically connected Cartesian grid consisted of hexahedral cells that could be deformed to body-fit complex shapes. A finite-volume method for a non-orthogonal grid was used to calculate the electromagnetic field. This method is based on Gedney-Lansing [1] and Madsen [2] algorithms, and is reduced to a standard FDTD algorithm for an orthogonal grid. Particle updates use current deposit formulation of Villasenor and Buneman [3] generalized to non-orthogonal meshes, preserving charge and current. The numerical stability of the electromagnetic algorithm was analyzed for a planar EM wave propagation in a distorted periodic box. The influence of face-to-edge transformation properties on the EM algorithm stability is analyzed. Energy conservation for a full PIC simulation of two-stream instability on non-orthogonal meshes is studied.			
14. SUBJECT TERMS electromagnetic, geometries, grid		15. NUMBER OF PAGES	
		16. PRICE CODE	
17. SECURITY CLASSIFICATION OF REPORT Unclassified	18. SECURITY CLASSIFICATION OF THIS PAGE Unclassified	19. SECURITY CLASSIFICATION OF ABSTRACT Unclassified	20. LIMITATION OF ABSTRACT UL

19981215 136

A Study of Stability and Energy Conservation of a 3-D Electromagnetic PIC Code for Non-Orthogonal Meshes.

Dmitri Kondrashov
California Institute of Technology, Pasadena
Joseph Wang, Paulett C. Liewer
JPL/California Institute of Technology, Pasadena

Summary

A 3-D electromagnetic particle-in-cell code (EMPIC) was developed for large-scale plasma simulation on parallel computers. To simulate plasma problems with complex geometries such as high-power microwave generation devices, curvilinear coordinates were used. A logically connected Cartesian grid consisted of hexahedral cells that could be deformed to body-fit complex shapes. A finite-volume method for a non-orthogonal grid was used to calculate the electromagnetic field. This method is based on Gedney-Lansing [1] and Madsen [2] algorithms, and is reduced to a standard FDTD algorithm for an orthogonal grid. Particle updates use current deposit formulation of Villasenor and Buneman [3] generalized to non-orthogonal meshes, preserving charge and current.

The numerical stability of the electromagnetic algorithm was analyzed for a planar EM wave propagation in a distorted periodic box. The influence of face-to-edge transformation properties on the EM algorithm stability is analyzed. Energy conservation for a full PIC simulation of two-stream instability on non-orthogonal meshes is studied.

Governing equations.

The EM fields in the code are computed from time-dependent Maxwell's equations in an integral form:

$$\begin{cases} \partial_t \int \mathbf{E} \cdot d\mathbf{s} = c \oint \mathbf{B} \cdot d\mathbf{l} + \int \mathbf{J} \cdot d\mathbf{s} \\ \partial_t \int \mathbf{B} \cdot d\mathbf{s} = -c \oint \mathbf{E} \cdot d\mathbf{l} \end{cases}$$

The particle trajectories are calculated from relativistic Newton's second law for a single charged particle in an electromagnetic field:

$$\begin{aligned} \partial_t \gamma m \mathbf{V} &= q \left(\mathbf{E} + \frac{\mathbf{V}}{c} \times \mathbf{B} \right) \\ \partial_t \mathbf{X} &= \mathbf{V} \end{aligned}$$

The EM algorithm is based on explicit DSI (discrete surface integral) solution of Maxwell's equations, tailored to the case of hexahedral grid cells. Particle trajectories are calculated by a standard leap-frog algorithm described in Birdsall and Langdon [4]. The code reduces to a standard orthogonal EMPIC code on Cartesian grid, (Wang, Liewer and Decyk, [5]).

Electromagnetic Algorithm Numerical Stability Study.

The algorithm uses a staggered grid system. The primary cell \mathbf{B} grid and dual cell \mathbf{E} grid are defined. The fundamental code variables are $\mathbf{B} \cdot d\mathbf{s}$ (on each face of \mathbf{B} grid cells), $\mathbf{E} \cdot d\mathbf{s}$ (on each face of \mathbf{E} cells), $\mathbf{B} \cdot d\mathbf{l}$ (on edges of the \mathbf{E} grid), and $\mathbf{E} \cdot d\mathbf{l}$ (on edges of the \mathbf{B} grid), Fig.1.

The integral Maxwell's equations are advanced using a 2nd order leap-frog scheme:

$$\begin{aligned} (\mathbf{E} \cdot d\mathbf{s})^{n+1} &= (\mathbf{E} \cdot d\mathbf{s})^n + \Delta t \left(c \sum_{\text{edges}} \mathbf{B} \cdot d\mathbf{l} + \mathbf{J} \cdot d\mathbf{s} \right)^{n+1/2} \\ (\mathbf{B} \cdot d\mathbf{s})^{n+3/2} &= (\mathbf{B} \cdot d\mathbf{s})^{n+1/2} - \Delta t c \left(\sum_{\text{edges}} \mathbf{E} \cdot d\mathbf{l} \right)^{n+1} \end{aligned}$$

The algorithm is completely specified with transformation from face quantities ($\mathbf{B} \cdot d\mathbf{s}$, $\mathbf{E} \cdot d\mathbf{s}$) to edge quantities. For a uniform grid this transformation is trivial, so that

$$\mathbf{B} \cdot d\mathbf{l} = \mathbf{B} \cdot d\mathbf{s} \left| \frac{d\mathbf{l}}{d\mathbf{s}} \right|$$

In this limit, a standard 2nd-order Yee algorithm is recovered. For a non-orthogonal grid, $d\mathbf{l}$ is not parallel to $d\mathbf{s}$, so additional work has to be done (Fig. 2, for a 2-D case). There, 5 $\mathbf{B} \cdot d\mathbf{s}$ values are needed to compute one $\mathbf{B} \cdot d\mathbf{l}$ value. To obtain $\mathbf{B} \cdot d\mathbf{l}$ at a particular cell face, say face 1 on Fig. 2, one first needs to find four B_{1i} ($i=2,5$) values at two vortices of the face 1 by solving linear system of equations:

$$\begin{aligned} B_{1i} \cdot d\mathbf{s}_1 &= (\mathbf{B} \cdot d\mathbf{s})_1 \\ B_{1i} \cdot d\mathbf{s}_i &= (\mathbf{B} \cdot d\mathbf{s})_i \end{aligned}, i=2-5.$$

where $(\mathbf{B} \cdot d\mathbf{s})_i$ ($i=1,5$) are known fundamental variables, and B_{1i} are unknown vectors. Next, a weighted average of B_{1i} is dotted with the dual-edge vector $d\mathbf{l}_1$ to form $\mathbf{B} \cdot d\mathbf{l}$:

$$(\mathbf{B} \cdot d\mathbf{l})_1 = \left(\sum B_{1i} \cdot \omega_{1i} \right) \cdot d\mathbf{l}_1$$

Here we can distinguish three different methods of weighting scheme:

Method A: Equal weights: $\omega_{1i} = 0.25$

Method B: Volume-based weights:

$$\omega_{li} = \frac{|ds_1 \times ds_i|}{\sum \omega_{li}}$$

Method C: Here $B \cdot dl$ is a sum along two line segments dl_{11} and dl_{12} from neighboring cell centers to cell face:

$$\begin{aligned} (B \cdot dl)_1 &= (B \cdot dl)_{11} + (B \cdot dl)_{12} \\ (B \cdot dl)_{11} &= (B_{12}\omega_{12} + B_{13}\omega_{13})dl_{11} \\ (B \cdot dl)_{12} &= (B_{14}\omega_{14} + B_{15}\omega_{15})dl_{12} \\ dl_1 &= dl_{11} + dl_{12} \end{aligned}$$

where weights are one-sided volume averaged. The purpose of Method C is to compute portions of edge values locally at each cell so that no interprocessor communication would be necessary. However, Method C has turned out to be the poorest one in terms of numerical stability.

Numerical Stability of the EM Algorithm.

The EM algorithm has been reported to have a weak numerical stability (Brandon and Rambo, [6]). Here the EM algorithm stability is analyzed on a test computation of a planar EM wave propagation through a distorted periodic box. Numerical parameters for a test case are as follows:

the wave is propagating along the z-axis,

number of grid points, $N_x=17$, $N_y=17$, $N_z=9$;

box dimensions, $L_x=10$, $L_y=10$, $L_z=20$;

speed of light $c=1$,

wave transient time is 20.

The grid is 2-D distorted in the x-y plane:

$$\begin{aligned} z(i, j, k) &= k \cdot h_z \\ x(i, j, k) &= i h_x + d \sin(m_x i h_x) \sin(m_y j h_y) \\ y(i, j, k) &= j h_y + d \sin(m_x i h_x) \sin(m_y j h_y) \end{aligned}$$

where h_x , h_y , h_z are mesh sizes for a uniform orthogonal grid,

$$m_x = \frac{2\pi}{L_x}, \quad m_y = \frac{2\pi}{L_y}$$

and d is distortion parameter. Examples of the distorted grid for several values of d are shown on Fig. Note that in this geometry the non-zero value of the z -component of $\mathbf{E} \cdot d\mathbf{s}$ represents numerical error, which makes it useful for analytical purposes. Logarithmic plots of total energy and maximum value of $(\mathbf{E} \cdot d\mathbf{s})_z$ over the computational domain as a function of time are shown in Fig. 4. Three methods of weighting scheme A, B and C are compared for a test run with $d=0.8$. All three methods are numerically unstable; Method A has the smallest growth rate, while method C has the highest one. Method A takes 7500, and method C 50 wave transient times to become unstable. One can observe that numerical error in z components of EM field directly affects numerical stability. Once the numerical error becomes comparable with the non-zero EM field components of exact solution, the instability appears as an exponential growth of total energy. The growth rate increases with distortion size (Fig. 5).

Langdon [7] suggested the importance of face-to-edge transformation properties for numerical stability. He considered a 2-D field in 2-D geometry and found that for the numerical stability, the face-to-edge transformation must be symmetric. In the 2-D case shown on Fig 2, it means that contribution of $(\mathbf{B} \cdot d\mathbf{s})_2$ to $(\mathbf{B} \cdot d\mathbf{l})_1$ must be equal to the contribution of $(\mathbf{B} \cdot d\mathbf{s})_1$ to $(\mathbf{B} \cdot d\mathbf{l})_2$.

Here the analysis for a 3-D DSI algorithm is presented. The discretized Maxwell's equations in an integral form can be written as

$$\begin{aligned} \dot{E}_{DF} &= S_E \cdot B_{DE} \\ \dot{B}_{PF} &= S_B \cdot E_{PE} \end{aligned}$$

where matrices S_E and S_B are related as

$$S_E = -S_B^T$$

and E_{DF} , B_{PF} , B_{DE} , E_{PE} are vectors of grid values of $\mathbf{E} \cdot d\mathbf{s}$, $\mathbf{B} \cdot d\mathbf{s}$, $\mathbf{B} \cdot d\mathbf{l}$ and $\mathbf{E} \cdot d\mathbf{l}$, respectively. The face-to-edge transformation can be specified as

$$\begin{aligned} B_{DE} &= T_B \cdot B_{PF} \\ E_{PE} &= T_E \cdot E_{DF} \end{aligned}$$

Using these definitions, we derive

$$\begin{aligned}\ddot{E}_{DF} &= -M_E E_{DF}, & M_E &= S_E T_B S_E^T T_E \\ \ddot{B}_{PF} &= -M_B B_{PF}, & M_B &= S_E^T T_E S_E T_B\end{aligned}$$

Thus, for computations to be stable numerically below Courant limit, matrices M_e and M_b must be symmetric and positive definite. In this case, all eigenvalues of M_e and M_b are positive. This requirement imposes restrictions on both T_e and T_b . In particular, if

$$S_E T_B = T_E^T S_E, \quad (1)$$

then M_e and M_b are symmetric. Let us consider several special cases.

1. Uniform Cartesian Mesh:

$$T_B = T_E = \Lambda \text{ (diagonal matrix)}$$

Clearly, the condition (1) is satisfied and solution is stable, which is known from the properties of the Yee algorithm.

2. Non-orthogonal uniformly skewed grid (Fig. 6):

Here we have symmetric face-to-edge transformation:

$$T_E = T_B = T_E^T$$

One can prove that condition (1) holds for such grid. Figure 7 shows that the solution is indeed numerically stable for a uniformly skewed grid.

3. General non-orthogonal grid, such as on Fig. 3:

Here condition (1) does not hold, so we can expect the solution to be numerically unstable. One can speculate that for different weighting schemes A, B and C, condition (1) holds to a different extent, which explains different results for numerical stability.

4. Langdon 2-D Field Analysis:

Langdon considered the case with

$$T_B = \Lambda$$

Thus, matrix M_b becomes : $M_B = S_E^T T_E S_E$, so for its symmetry T_e must be symmetric. However, this is a special case. But in general, condition (1) must be satisfied for numerical solution to be stable. Condition (1) imposes that for a 3-D field, even a symmetric transformation does not guarantee numerical stability.

Test Case for a Full PIC Simulation on Non-Orthogonal Meshes.

Let us consider a counter-streaming beam system: two equal electron beams are set to move at different directions with opposite velocities $V_d=0.4c$. The electrons within each beam have Maxwellian distribution with thermal velocity $v_{th}=0.05c$. The ions are considered to be a fixed background. This counter-streaming system generates the well-known two-stream instability. Calculation is again performed in a distorted periodic box as described earlier. In Fig. 8 electromagnetic energy, particle kinetic energy and total energy in the system are plotted as functions of time for distorted and undistorted grids. Figure 8 shows that calculations correctly predict energy transfer between the particles and the fields which results from instability excitation and saturation. The total energy remains constant, as it should be. The error in total energy conservation does not exceed 2% even for a highly distorted grid (Fig. 9), and it decreases with increased number of particles (Fig. 10). The EM numerical instability plays no role in this computation as the characteristic time of the calculation is only several transient wave times.

References

- [1] S. Gedney and F. Lansing, "A Generalized Yee-Algorithm for the Analysis of Microwave Circuit Devices", submitted to *IEEE Trans. Microwave Theory and Techniques* (1995).
- [2] N.K. Madsen, "Divergence Preserving Discrete Surface Integral Methods for Maxwell's Curl Equations Using Non-Orthogonal Unstructured Grid", *J. Comp. Phys.*, 119: 34-35 (1995).
- [3] J. Villasenor and O. Buneman, "Rigorous Charge Conservation for Local Electromagnetic Field Solvers", *Comp. Phys. Comm.*, 69: 306-316 (1992).
- [4] C.K. Birdsall and A.B. Langdon, *Plasma Physics via Computer Simulation*, McGraw-Hill, New York, 1985.
- [5] J. Wang, P. Liewer, V. Decyk, "3-D Electromagnetic Plasma Particle Simulations On a MIMD Parallel Computer", *Comp. Phys. Comm.*, 87: 35-53 (1995).
- [6] S.T. Brandon and P.W. Rambo, "Stability of the DSI Electromagnetic Update Algorithm on a Chevron Grid." 22nd IEEE International Conference on Plasma Sciences, June 1995.
- [7] A.B. Langdon, "2-D Electromagnetic and PIC on a Quadrilateral Mesh", Memorandum No.UCB/ERLM95/96, College of Eng., Univ. California, Berkeley, Dec. 1995.

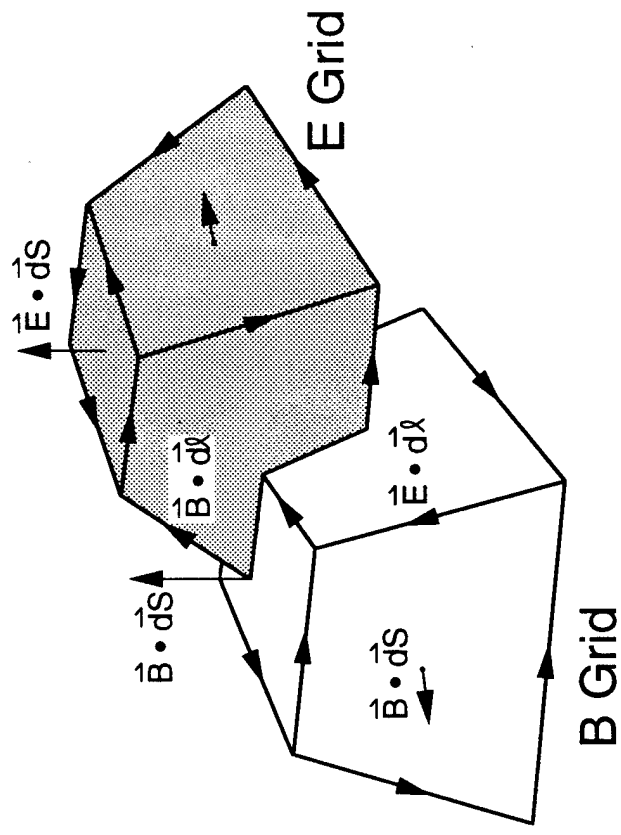


Fig.1 Dual and primary grid cell layout.

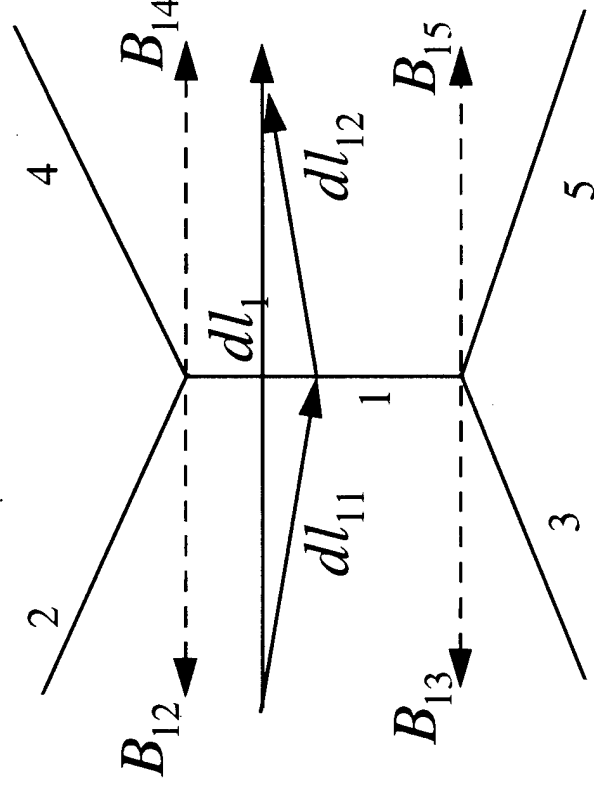
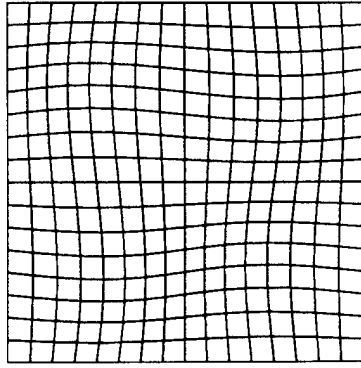
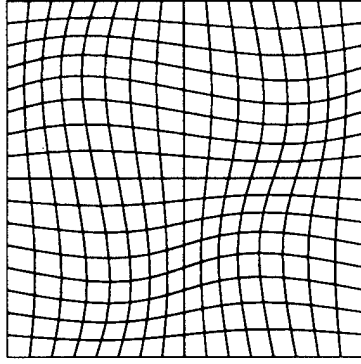


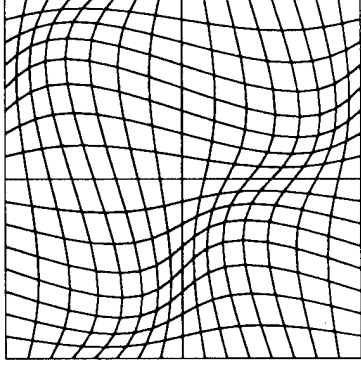
Fig.2 Face-to-edge transformation on 2-D grid.



$d=0.2$



$d=0.4$



$d=0.8$

Fig.3 2-D distorted grid

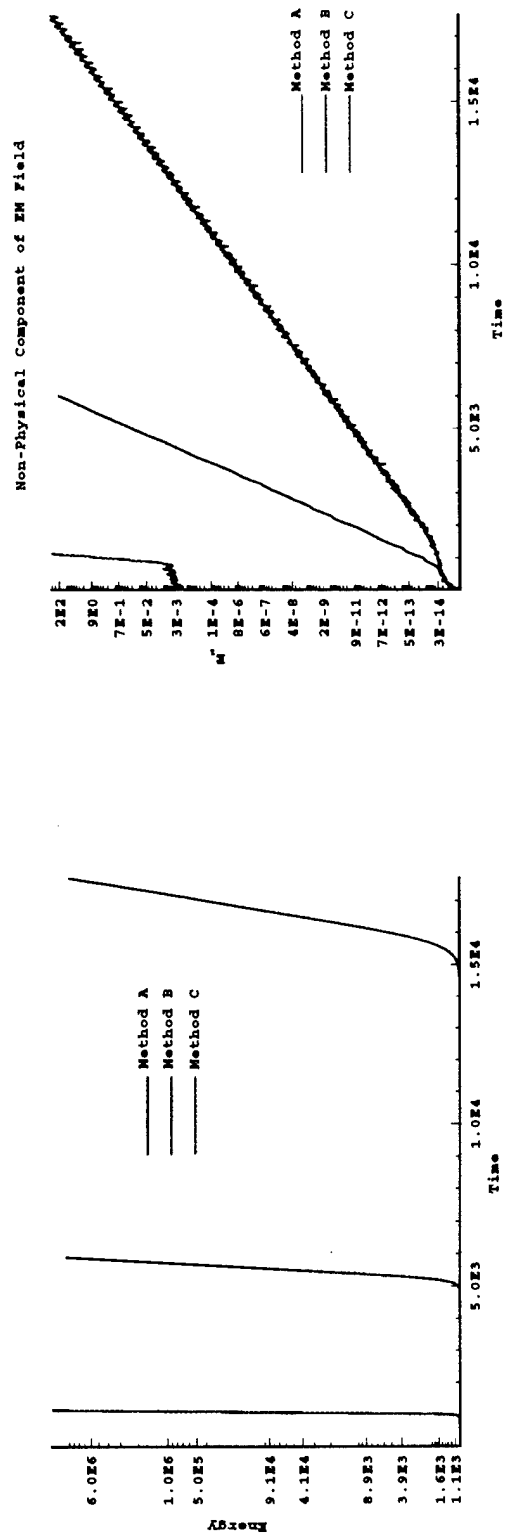
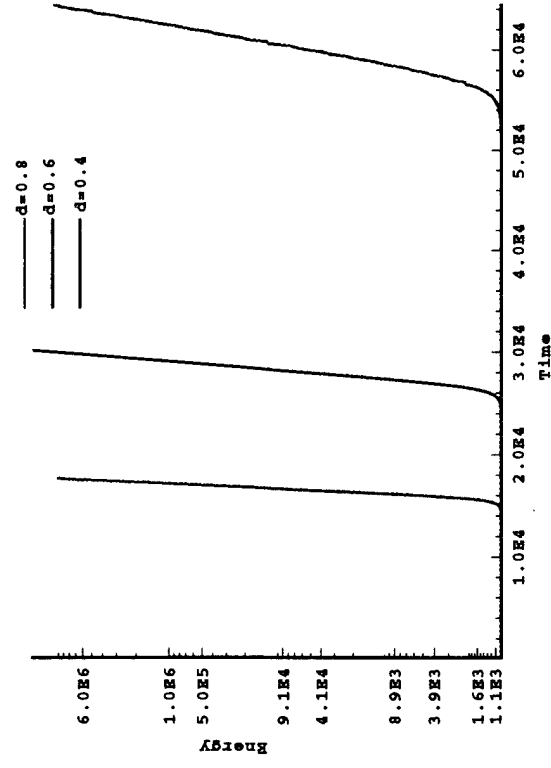


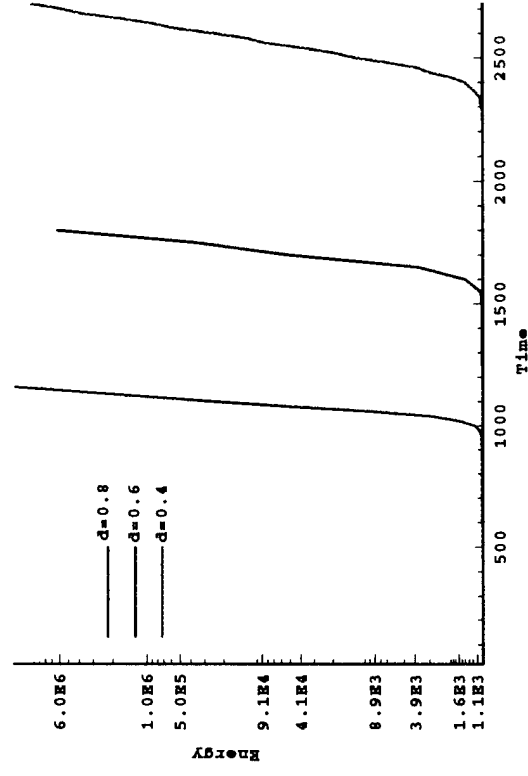
Fig.4 Total energy and non-physical component of EM field in numerical stability test case.

Fig.5 Best and worst transformation method for
numerical stability

Method A



Method C



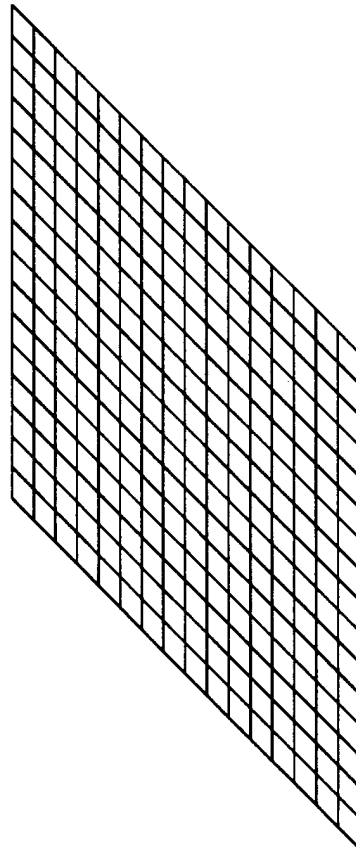


Fig.6 Uniformly skewed
Grid.

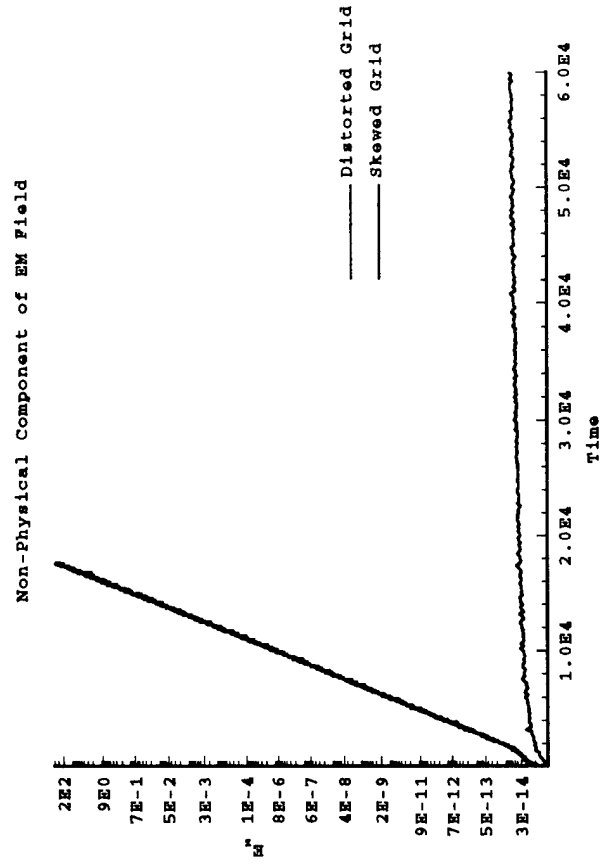
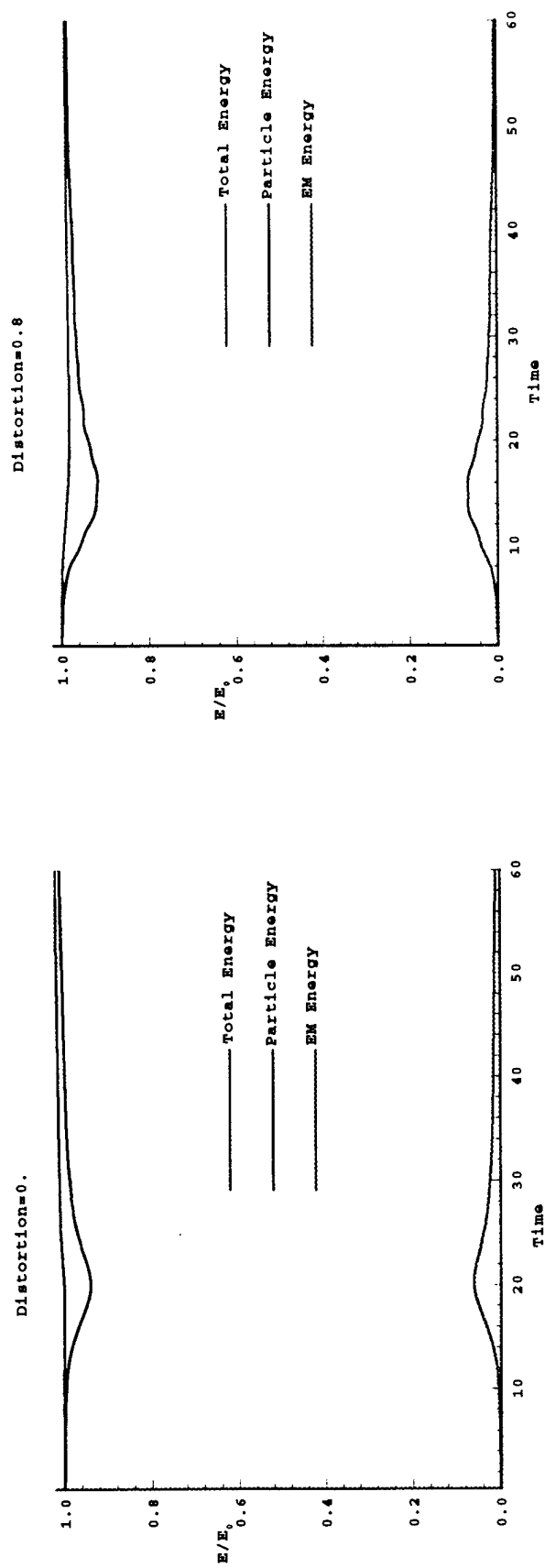


Fig.7 Numerical stability
for uniformly skewed grid.

Fig.8 Two-stream instability test case:energy
timehistory



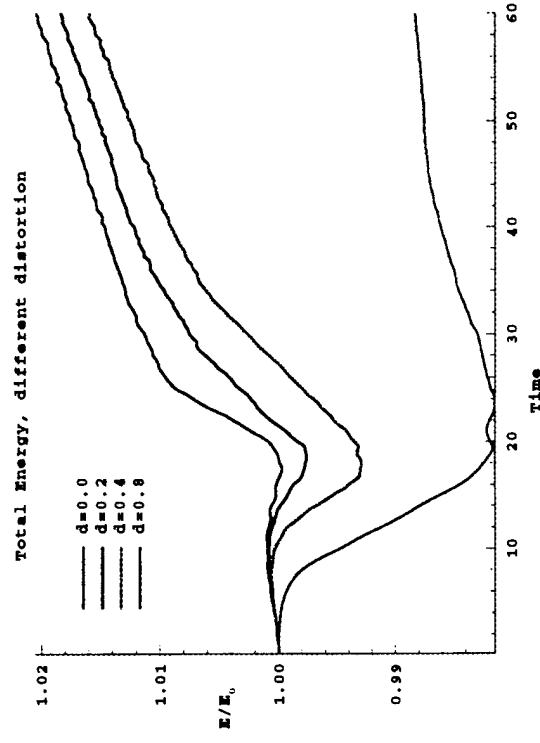


Fig.9 Error in total energy conservation for different distortions.

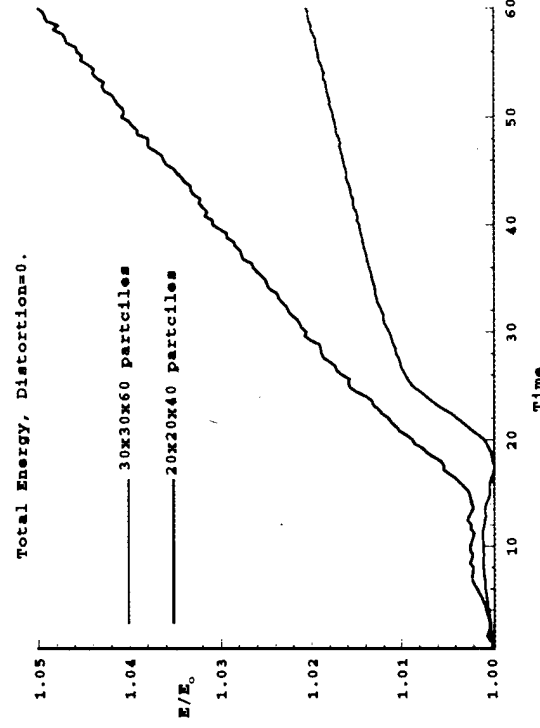


Fig.10 Error in total energy conservation for different number of particles.